Journal of Hydrology: Regional Studies 26 (2019) 100637

Contents lists available at ScienceDirect

Journal of Hydrology: Regional Studies

journal homepage: www.elsevier.com/locate/ejrh

Regional hydro-climatic changes in the Southern Amazon Basin (Upper Madeira Basin) during the 1982–2017 period

Jhan Carlo Espinoza[a,*], Anna A. Sörensson[b,c], Josyane Ronchail[d], Jorge Molina-Carpio[e], Hans Segura[a], Omar Gutierrez-Cori[f], Romina Ruscica[b,c], Thomas Condom[a], Sly Wongchuig-Correa[a,g]

[a] Univ. Grenoble Alpes, IRD, CNRS, Grenoble INP, Insitut des Géosciences de l'Environnement (IGE, UMR 5001), 38000, Grenoble, France
[b] Universidad de Buenos Aires - Consejo Nacional de Investigaciones Científicas y Técnicas, Centro de Investigaciones del Mar y la Atmósfera (CIMA/UBA-CONICET), Buenos Aires, Argentina
[c] Institut Franco-Argentin d'Etudes sur le Climat et ses Impacts, Unité Mixte Internationale (UMI-IFAECI/CNRS-CONICET-UBA), Argentina
[d] Univ. Paris Diderot and Université de Paris, UMR LOCEAN (Sorbonne Universités-UPMC, CNRS, IRD, MNHN), Paris, France
[e] Instituto de Hidráulica e Hidrología (IHH), Universidad Mayor de San Andrés, Campus Universitario, Calle 30 Cota Cota, La Paz, 15000, Bolivia
[f] Laboratorie de Météorologie Dynamique (LMD), Institut Pierre Simon Laplace- IPSL (Sorbone Université, CNRS), Paris, France
[g] Instituto de Pesquisas Hidráulicas IPH, Universidade Federal do Rio Grande do Sul UFRGS, Porto Alegre, Brazil

ARTICLE INFO

Keywords:
Runoff coefficient
Rainfall trends
Atmosphere and land surface interactions

ABSTRACT

Study region: Upper Madeira Basin (975,500 km^2) in Southern Amazonia, which is suffering a biophysical transition, involving deforestation and changes in rainfall regime.
Study focus: The evolution of the runoff coefficient (Rc: runoff/rainfall) is examined as an indicator of the environmental changes (1982–2017).
New hydrological insights for the region: At an annual scale, the Rc at Porto Velho station declines while neither the basin-averaged rainfall nor the runoff change. During the low-water period Rc and runoff diminish while no changes are observed in rainfall. This cannot be explained by increase of evapotranspiration since the basin-averaged actual evapotranspiration decreases. To explain the decrease of Rc, a regional analysis is undertaken. While the characteristic rainfall-runoff time-lag (CT) at Porto Velho basin is estimated to 60 days, CT is higher (65–75 days) in the south and lower (50 days) over the Amazon-Andes transition regions. It is found that 1) the southern basin (south of 14 °S) best explains low-level Porto Velho runoff, 2) in the south, rainfall diminishes and the frequency of dry days increases. Both features explain the diminution of the runoff and the Rc in Porto Velho. Moreover, the increasing dryness in the south compensates for the rainfall and frequency of wet days (> 10 mm) increase north of 14 °S and explains the lack of basin-averaged rainfall trends of the upper Madeira basin.

1. Introduction

The upper Madeira Basin at Porto Velho extends over 975,500 km^2 and is characterized by an altitude variation from 50 to 6450 masl, setting the scene for a wide range of climatic, geomorphological and biological features. The hydrological basin at Porto Velho station (mean annual discharge of 18,300 m^3/s; Molina-Carpio et al., 2017) extends in Peru (11% of its surface), in Bolivia (73%) and in Brazil (16%). The basin is divided into four main geomorphological units: the Andes, the Brazilian shield, the Amazon plain and

* Corresponding author.
E-mail address: jhan-carlo.espinoza@ird.fr (J.C. Espinoza).

https://doi.org/10.1016/j.ejrh.2019.100637
Received 10 June 2019; Received in revised form 29 September 2019; Accepted 25 October 2019
Available online 21 November 2019

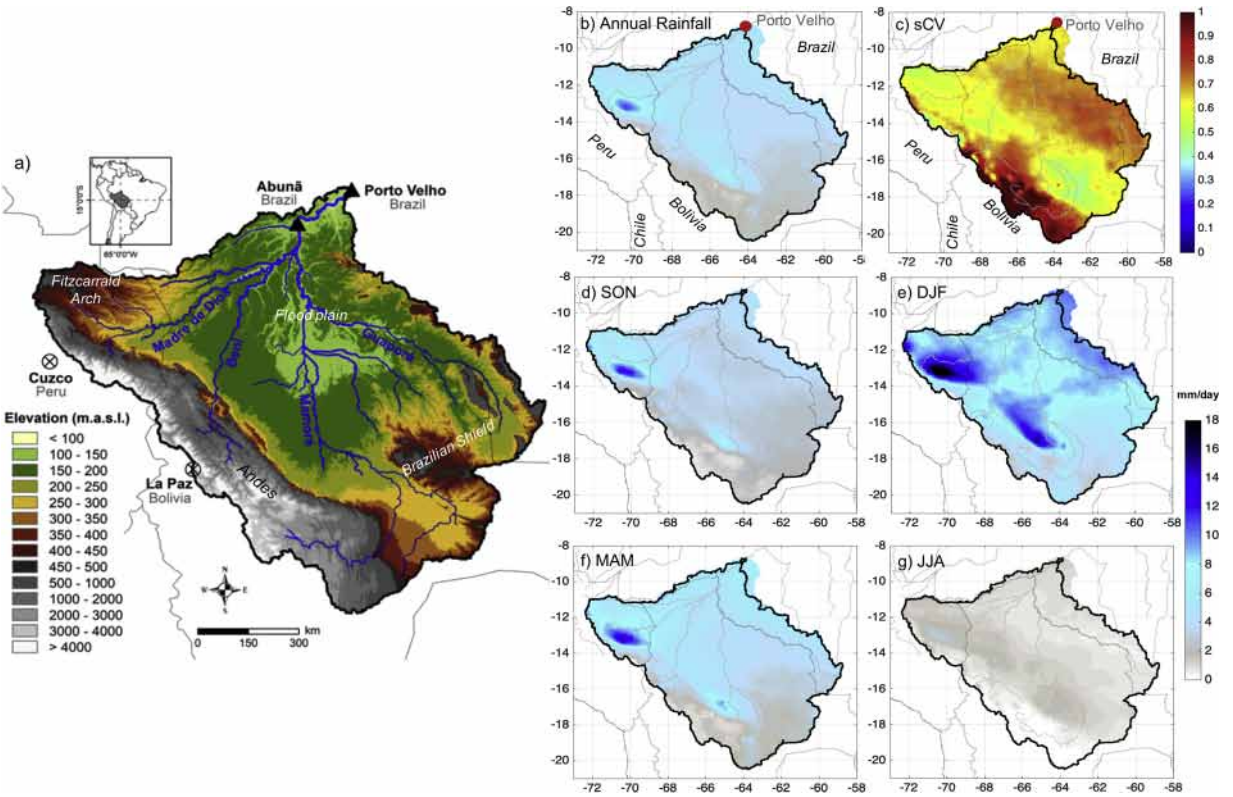

Fig. 1. a) Main rivers (blue lines) and topography (40–4000 masl) of the upper Madeira Basin. Black triangles indicate the hydrological station: Porto Velho (8.75 °S, 63.92 °W) and Abunã (9.70 °S, 65.36 °W). Main cities and countries are indicated. The topography and the hydrological network were computed using SRTM at 90 m of resolution. b) Mean annual rainfall (in mm/day) over the upper Madeira Basin. c) The seasonal variation coefficient (sVC, defined as the ratio of the standard deviation of the annual cycle of precipitation divided by the annual mean). d) to g) Three-monthly mean of daily rainfall (in mm/day) considering September to November (SON), December to February (DJF), March to May (MAM) and June to August (JJA), respectively. From b to g panels, main rivers and limit of the countries are shown in grey lines and the delimitation of the upper Madeira Basin in black lines. CHIRPS rainfall data is used at 0.05°x0.05° of resolution for the 1982–2017 (1981–2017) period in panels b, c and e (d, f and g).

the Fitzcarrald Arch formation (Fig. 1a). The Madeira river basin at Porto Velho station consists of four main tributaries: Madre de Dios arriving from the Peruvian Andes, Beni and Mamoré from the central Bolivian Andes and the Guaporé River from the south-eastern part of the basin (Brazilian Shield). While the Andes cover around 23% of the upper Madeira surface, a vast floodplain, the Llanos de Mojos, extends over the lowlands between the Beni, Mamoré and Guaporé rivers (Guyot, 1993, 1996). The Llanos de Mojos floodplain is characterized by a mean altitude of 150 masl, a slope of less than 10 cm/km (Guyot, 1993) and a floodable surface up to 150,000 km^2 (Hamilton et al., 2004; Ovando et al., 2016; Parrens et al., 2019, among others).

Rainfall over the upper Madeira Basin shows a strong spatial variability, with average annual values of around 1800 mm/year or 5 mm/day while lower values are observed in the southernmost part of the basin and over the Andes (Fig. 1b; Roche et al., 1990; Molina-Carpio et al., 2017). The Andes/Amazon transition region of the upper Madeira Basin is among the rainiest regions of the world, characterized by the interactions between large-scale winds circulation and the topography that determine a complex rainfall distribution (e.g. Killeen et al., 2007; Bookhagen and Strecker, 2008; Espinoza et al., 2009a). Orographic effects and exposure to easterly winds produce a strong annual rainfall gradient between the lowlands and the Andes that can reach 190 mm/km. Indeed, "rainfall hotspot" regions with 4000 to 6000 mm/year (~12-16 mm/day) are identified at low elevations in the Andean foothills (400–700 masl) and in windward conditions (e.g. Espinoza et al., 2015; Junquas et al., 2018). These very wet regions are observed particularly over the upper Madre de Dios, Beni and Mamoré rivers (Fig. 1). Based on the 1968–1982 period, Roche (1990) used empirical equations and estimated the surface water balance at an annual scale over the upper Madeira Basin, obtaining an average precipitation of 4.98 mm/day, a mean runoff at Porto Velho of 1.78 mm/day and a mean evapotranspiration of 3.21 mm/day. Computing the surface water balance with evapotranspiration data from different sources, Builes-Jaramillo and Poveda (2018) show a state close to balance within a ± 10% tolerance in the Madeira Basin. However, a large negative residual is reported in the upper Beni River at Rurrenabaque station, probably related to uncertainties in evapotranspiration products (Sörensson and Ruscica, 2018; Getirana et al., 2014) and underestimation of rainfall over the Amazon-Andes transition region (Espinoza et al., 2015).

The southern Amazon Basin, including the upper Madeira, is characterized by a wet season in the austral summer (December-March), related to the presence of the South Atlantic Convergence Zone (SACZ) during the mature phase of the South America

Monsoon System (SAMS) (e.g Vera et al., 2006; Marengo et al., 2012). In absence of the SAMS, a marked dry season predominates during the austral winter (June-August). In terms of basin average, over 50% of the annual rainfall is recorded between December-March (e.g. Roche, 1990; Ronchail and Gallaire, 2006). However, over the rainfall hotspot region in the upper Madre de Dios Basin, exceptional rainfall also occurs during the austral dry season, estimated to be around 1000 mm during June-August in the San Gabán meteorological station (Espinoza et al., 2015). Rainfall seasonality drives runoff and terrestrial water storage (TWS) variability over the basin. Indeed, Molina-Carpio et al. (2017) shows a time-lag of two month between basin averaged rainfall and runoff at Porto Velho. In addition, using satellite information of TWS from Gravity Recovery and Climate Experiment (GRACE, at 1°x1° of resolution), a time-lag of two months has been detected between rainfall and TWS in the Madeira basin (e.g. Xavier et al., 2010; Frappart et al., 2013) with a seasonal range of around 4–5 mm/day (Azarderakhsh et al., 2011).

Recent studies have documented an intensification of the seasonal extreme hydrological events over the Amazon Basin (e.g. Marengo and Espinoza, 2016; Barichivich et al., 2018; Espinoza et al., 2019). In the Madeira Basin, severe flooding occurred, for instance in 1992, 1993, 1997 (Ronchail et al., 2005; Bourrel et al., 2009), 2007, 2008 and recently, exceptional rainfall and discharge values were reported in 2014 (Espinoza et al., 2014; Ovando et al., 2016), which do not always coincide with those that occurred in the main stem of the Amazon River (Molina-Carpio et al., 2017). In terms of hydrological impacts, large floods are also intensified by the superimposition of flood waves from major tributaries of the upper Madeira River (Ovando et al., 2016).

Several studies have reported that discharge during the low-water season in the southwestern Amazon, including the Porto Velho station, exhibited a significant decrease during the last four decades (Espinoza et al., 2009b; Lopes et al., 2016; Molina-Carpio et al., 2017; Wongchuig-Correa et al., 2017). In the southern part of the Amazon Basin, a longer (shorter) dry (wet) season has been reported, specifically since the 1980s (e.g. Salazar et al., 2007; Marengo et al., 2011; Saatchi et al., 2013; Fu et al., 2013; Arias et al., 2015; Debortoli et al., 2015). In a recent study, Espinoza et al. (2019) documented a significant increase of the dry-day frequency (DDF) for the 1981–2017 period, particularly over the Bolivian Amazon during the beginning of the wet season (September-November). In addition, future climate scenarios suggest that this region could suffer an intensification of extreme droughts (Boisier et al., 2015; Guimberteau et al., 2013; Polade et al., 2014).

In addition to the above described changes in rainfall intensity over southern Amazonia, recent modeling studies suggest that southern Amazonia is suffering a process of biophysical transition. Two possible “tipping points” have been identified, associated with temperature increase of 4 °C or with deforestation exceeding 40% of the forest area. Surpassing these “typing points”, large-scale “savannization” of almost the entire southern and eastern Amazon, including Madeira Basin, may take place (Nobre et al., 2016). Indeed, a fragile hydrological equilibrium has been identified in southern Amazon, which can be broken during drought events producing persistent changes in rainforest canopy structure (Maeda et al., 2015). Total deforestation in Amazonia now reaches 20% of the area and is particularly extended over the “Arc of Deforestation” in the southern and southwestern Amazonia (Nobre et al., 2016). These environmental changes could substantially impact the hydrological cycle in the southwestern Amazon Basin, where the recycling of water from the central and eastern Amazon rainforest is particularly significant (Zemp et al., 2017; Sumila et al., 2017; Staal et al., 2018; Marengo et al., 2018).

That is, both climatic and environmental changes in southern Amazonia during the last four decades have been established by the above-mentioned scientific literature. An important indicator of environmental changes in a basin, frequently used in hydro-climatic studies, is the runoff coefficient (Rc: runoff/rainfall), which embeds climate and/or land use changes (e.g. Xu et al., 2018). In this study, we aim to assess the evolution of the runoff coefficient for the 1982–2017 period in the upper Madeira Basin. Annual and seasonal Rc is analyzed in relation to the spatio-temporal variability of the main components of the hydrological cycle, rainfall and evapotranspiration. The description of the hydroclimatic data and statistical methods is proposed in Sections 2 and 3, respectively, and the long-term surface water balance for the upper Madeira Basin is calculated in Section 4. With the aim of depicting the Rc evolution over the basin, the interannual evolution of both basin-averaged rainfall and runoff at Porto Velho station is analyzed in Section 5. Given the geomorphological and climatic complexity of the upper Madeira basin, we seek to understand how the regional variability of precipitation within the basin can affect the evolution of Rc (Section 6). To this end, Section 6.1 is devoted to analyze spatial variations in the characteristic rainfall-runoff time-lag in the basin and how this feature may affect the seasonal relationship between regional precipitation and runoff at Porto Velho. Regional trends in precipitation are analyzed in Section 6.2 to understand how changes in regional precipitation can affect Rc variability over the basin. Finally, concluding remarks are presented in Section 7.

2. Hydro-climatic data

2.1. Runoff time series in the upper Madeira Basin

In this study daily runoff (R) discharge data is analyzed on the upper Madeira River at Porto Velho and Abunã hydrological stations, covering drainage areas of 975,500 km^2 and 920,100 km^2, respectively (Fig. 1a). Daily discharge time series were provided by the Brazilian Water National Office (Agencia Nacional de Águas – ANA) and quality control was checked by the SNO-HYBAM observatory (for more details see Molina-Carpio et al., 2017). Discharge data used in this study corresponds to the 1981–2017 period. However, due to missing values, annual and June-July discharges in 2011 at Porto Velho are not taken into account and 1992, 1999–2001 annual values in Abunã are removed from our analysis. In order to compare the discharge with other hydrological variables, discharge is converted to daily runoff (mm/day) for both stations.

2.2. Daily rainfall datasets

2.2.1. The Climate Hazards Group Infrared Precipitation with Stations (CHIRPS)

The CHIRPS daily precipitation (*P*) dataset is based on global cold cloud duration as a primary source for calculating precipitation at a global scale. Then, these estimations are calibrated with the precipitation estimated from the TRMM-3B42 V7 product and rainfall data from the global rain gauges network. Finally, a high spatial resolution rainfall dataset is provided at $0.05^\circ \times 0.05^\circ$ of horizontal resolution (Funk et al., 2015). In this study, the original resolution of CHIRPS is used for the 1981–2017 period. This information is available at http://chg.geog.ucsb.edu/data/chirps/.

2.2.2. Interpolated HYBAM observed precipitation data (HOP)

Daily HOP rainfall data set is based on 752 rain gauges provided by national agencies responsible for hydro-meteorological monitoring in the Amazonian countries: ANA in Brazil, SENAMHI in Peru and Bolivia, INAMHI in Ecuador and IDEAM in Colombia (Espinoza et al., 2009a; Guimberteau et al., 2012). HOP data is spatially interpolated to a $1^\circ \times 1^\circ$ horizontal resolution. For more details about the ability of the interpolated HOP data to reproduce hydrological variability in the Amazon River, see Guimberteau et al. (2012) and Guimberteau et al. (2013). Satellite-based precipitation products like CHIRPS have been validated in the Amazon Basin with the HOP data set, at interannual and intraseasonal time-scales, and also for the daily rainfall extremes by Wongchuig-Correa et al. (2017); Paccini et al. (2017); Espinoza et al. (2019), among others. Daily-interpolated HOP data are freely available in NetCDF format on the http://www.ore-hybam.org web site.

2.3. Evapotranspiration

We use the actual evapotranspiration (E) product GLEAMv3.2a (Miralles et al., 2011; Martens et al., 2017, downloaded from https://www.gleam.eu/#downloads). GLEAM (Global Land Evaporation Amsterdam Model) estimates the potential evapotranspiration through the Priestly and Taylor equation and uses a set of algorithms that calculates the different components of E separately (transpiration, interception, bare soil, open-water evaporation and sublimation) using meteorological and vegetation data as input. The precipitation input to GLEAMv3.2a is MSWEP v1.0 (Beck et al., 2017), which is a multisource merged product based on in situ, remote sensed and reanalysis data. Four types of land covers are possible in GLEAMv3.2a: bare soil, low vegetation, tall vegetation and open water. The vegetation cover is produced using the MODIS product MOD44B and is therefore static. However, the variations in vegetation status is considered in the stress-factor (used to convert potential E to actual E) which is based on remote sensed Vegetation Optical Index from CCI-LPRM (Liu et al., 2013) and soil moisture both from remote sensing (ESA CCI SM v2.3, Liu et al., 2012) and land-reanalysis (GLDAS Noah, Rodell et al., 2004) products assimilated into the GLEAM multi-layer soil model. The upper Madeira Basin belongs to the southern Amazon region where the uncertainty of gridded E estimates from different sources such as remote sensing data and land reanalysis is high (Sörensson and Ruscica, 2018), in part because of lack of basic understanding of the processes governing E in this region (Christoffersen et al., 2014; Getirana et al., 2014; Sun et al., 2019). However, since we study a closed basin, we are able to choose the E dataset that best closes the annual water-budget (comparing rainfall to addition of runoff and E) for the period 1982–2017 (not shown).

2.4. Terrestrial water storage from the GRACE Mission

The equivalent water thickness estimated by the GRACE data is used as proxy of the TWS in the upper Madeira Basin. The GRACE consists of twin satellites that measure changes in the Earth's gravity field due to displacement of water, air or land masses. Many studies have shown the capacity of GRACE to depict continental water storage variations at large spatial scales (Tapley et al., 2004; Ramillien et al., 2008) as well as for validation purposes into hydrological models (Getirana et al., 2011; Paiva et al., 2013; Siqueira et al., 2018). It is important to note that the equivalent water thickness values are not absolute values of water storage. In fact, these are anomalies relative to the 2004–2009 time-mean baseline (Swenson and Wahr, 2006). In this study, we use the RL05 Level-3 version of monthly time-variable gravity data with spherical harmonic coefficients up to one degree, which has a spatial resolution of $\sim 1^\circ$x $\sim 1^\circ$ with a monthly time step. We use three (3) products of equivalent water thickness, all based on the GRACE gravimeter raw data, but developed by different research centres and laboratories: The Jet Propulsion Laboratory (JPL), the University of Texas Center for Space Research (CSR) and the GeoForschungsZentrum (GFZ) Potsdam. The RL05 data used in this work are 159-month CSR, JPL and GFZ data from April 2002 to January 2017. The data are available at https://podaac.jpl.nasa.gov/dataset/TELLUS_LAND_NC_RL05. In this study, we use the term TWS as the mean of equivalent water thickness from the three products, as recommended by Sakumura et al. (2014), spatially averaged over the upper Madeira Basin at Porto Velho station. Thus, changes in TWS represent the basin-average change in water storage over the basin on a monthly time scale. For more details about the GRACE data and their applications in the Amazon Basin, see Papa et al. (2008); Chen et al. (2010); Xavier et al. (2010); Frappart et al. (2012, 2013), among others.

2.5. Topography data from digital elevation model (DEM)

In this study, we use the freely available 90 m DEM from the Shuttle Radar Topography Mission (SRTM-V4.1) (Farr et al., 2007) available at http://srtm.csi.cgiar.org/srtmdata/. This information has been used to determine landscape morphology, the main fluvial network, the longitudinal slopes of the main rivers, and the distance of each point of the river to the Porto Velho station.

A summary of the dataset used to assess the regional hydro-climatic changes in the Southern Amazon Basin is presented in Table S1.

3. Statistical methods

Linear correlation is conducted in order to analyze the relationship between rainfall and runoff. For this purpose, the parametric Pearson coefficient (r) is computed using significance at least at $p < 0.05$. The seasonal variation coefficient (sVC) of rainfall, defined as the ratio of the standard deviation of monthly values to the mean of monthly values (1982–2017), was also calculated for each of the grid-points defined by CHIRPS. High (low) values of sVC represent strong (weak) rainfall seasonality, i.e. high (low) differences between dry and wet seasons (Espinoza et al., 2009a).

The characteristic rainfall-runoff time-lag over the basin is an indicator of the mean travel time of the streamflow wave through the catchment. This characteristic time-lag (CT) is defined as the time-lag of runoff (in days) necessary to obtain the maximum coefficient of correlation between rainfall and runoff. CT is obtained maximizing r in: $r(P_i, R_{i+CT})$; where r is the Pearson coefficient of correlation between P and R; P_i is rainfall on the day i, and R_{i+CT} is the runoff on the day i considering a lag of CT days. In addition, the runoff coefficient ($Rc = R/P$) is defined as the ratio between runoff observed in a hydrological station (in this study Porto Velho or Abunã) and the spatially averaged rainfall over the basin. Rc is analyzed at annual and seasonal time scales.

Finally, in order to compute the interannual evolution of the hydro-climatic variables, trends and break points are analyzed in the September-to-August (November-to-October) annual averages of P (R). To identify trends in the hydroclimatic time series, we use rank-based non-parametric Kendall test (τ; Kendall, 1975). Breaks and changes in the series are evaluated using the Pettitt method (Pettitt, 1979), a non-parametric test based on changes in the average and the range of the time series subdivided into sub-series. These methods have been applied widely in hydroclimatologic studies and are considered among of the most complete tests for time series analysis (e.g. Zbigniew, 2004).

4. Seasonality and long-term trends of the surface water balance

The wet season in the upper Madeira Basins coincides with the mature phase of the SAMS from December to March, with mean rainfall values higher than 6 mm/day over the 1982–2017 period (blue line in Fig. 2). Fig. 1b displays the mean annual rainfall values, while the strength of the seasonal cycle can be described with the seasonal coefficient of variability (sCV) displayed in Fig. 1c. Maximum daily rainfall occurs during December through February especially during January and February over the upper part of the Madre de Dios, Beni and Mamoré basins, characterized by the presence of rainfall "hotspot" regions, where more than 16 mm/day are reported (Fig. 1e). Dry conditions are clearly identified during June-August season (around 1 mm/day at a basin average scale, Fig. 2 and Table 1). During this season, rainfall is near to zero in the Andean part of the basin (higher than 3000 masl), around 2 mm/day in the lowlands and around 1 mm/day in the upper Guaporé Basin (Fig. 1g). In the upper Madre de Dios Basin, however, rainfall can reach 9 mm/day in the Peruvian hotspot as reported in previous studies (see introduction). sCV is high over the Bolivian Andean region ($sCV > 0.9$) and over the lower Guaporé and Mamoré rivers ($sCV > 0.7$). Low sCV values are observed over the Amazon-Andes transition region ($sCV < 0.6$), probably related to the presence of the intense rainfall over the hotspot regions noticeable during all the seasons (Fig. 1d–g). At an annual scale, the mean rainfall value over the upper Madeira Basin, computed for the 1982–2017 period, is 4.27 mm/day (Table 1).

Associated with the above described rainfall regime, runoff annual cycle in Porto Velho shows maximum (minimum) values between March-April (September-October), approximately two months after the respective maximum and minimum rainfall values (black line in Fig. 2). According to Table 1, runoff values vary from 0.52 mm/day (in August-October) to 3.09 mm/day (in February-April) and the mean annual value is estimated in 1.71 mm/day. Based on these values, the mean annual runoff coefficient (Rc) estimated in the upper Madeira Basin for the 1982–2017 period is 0.40 (Table 1). At the seasonal scale, Rc varies from 0.39 and 0.40

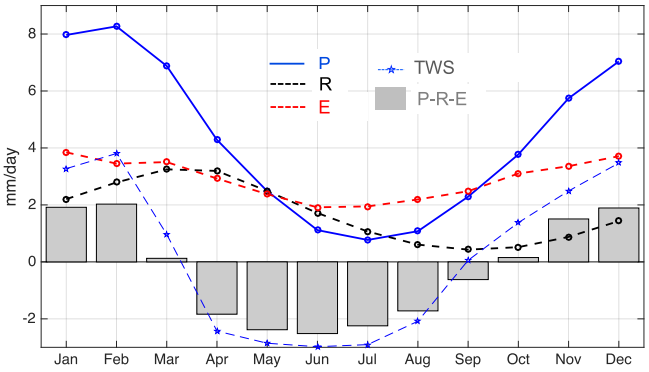

Fig. 2. Mean annual cycles of rainfall (P, blue line), runoff (R, black line) at the Porto Velho station, actual evapotranspiration (E, red line) and monthly changes in terrestrial water storage (TWS, dotted blue line) spatially averaged over the upper Madeira Basin. P, R and E are computed for the 1982–2017 period and TWS for the 2002–2017 period. The monthly difference of P-R-E is displayed in grey bars.

Table 1
Annual and three-monthly mean values of rainfall (P) and evapotranspiration (E) spatially averaged over the upper Madeira Basin and runoff (R) at Porto Velho. Runoff coefficient (Rc) is the ratio R/P. In the left column, the first couple of months corresponds to P and E, while the couple of months between parenthesis corresponds to R. r(x,y) means the Pearson coefficient of correlation between variables x and y, τ(x) means the τ coefficient resulting from the Kendall trend test in the x time series and Pett (x) means the year when a break points is identified by the Pettitt test of the time series of x. Only values with $p < 0.1$ are indicated in correlation, trend and break analysis. Values significant at $p < 0.05$ ($p < 0.01$) are underlined and in italic (bold). Years in red color means that a diminution is reported after the break point. The analyzed time period is 1981–2017, with exception of December-February and annual time series where analyses are computed for the 1982–2017 period.

	P(mm/d)	R(mm/d)	Rc	E(mm/d)	r(P,R)	r(P,Rc)	r(R,Rc)	τ(P)	τ(R)	τ(Rc)	τ(E)	Pett(P)	Pett(R)	Pett(Rc)	Pett(E)
Mean Annual	4.27	1.71	0.40	2.90	**0.71**	---	**0.86**	---	---	*-0.23*	**-0.31**	---	---	*1998*	*1995*
Sept-Nov (Nov-Jan)	3.94	1.52	0.39	2.98	**0.73**	---	**0.80**	---	*-0.26*	---	---	---	---	---	---
Dec-Feb (Feb-Apr)	7.68	3.09	0.40	3.66	**0.56**	---	**0.72**	---	---	---	**-0.56**	---	---	---	*1997*
Mar-May (May-Jul)	4.55	1.76	0.39	2.94	**0.70**	---	**0.87**	---	---	---	---	---	---	---	*1995*
Jun-Agu (Agu-Oct)	0.99	0.52	0.53	2.02	**0.45**	---	**0.71**	---	*-0.24*	*-0.26*	---	---	*1993*	*1997*	---

in the transitional and wet season respectively, to 0.53 in the dry season; however, annual Rc is closer to Rc during the wet season, probably related to the weight of this season in the annual water balance. The same analysis is carried out for mean annual rainfall and runoff at Abunã station (upstream of Porto Velho station, Fig. 1a), where Rc is estimated to 0.38. At the scale of the upper Madeira Basin at Porto Velho, these results are slightly higher than those provided for the 1968–1982 period by Roche (1990), where a Rc of 0.35 is estimated, with mean rainfall and runoff values of 4.98 mm/day and 1.78 mm/day, respectively. Both rainfall and runoff are higher in Roche et al (1990), particularly the former, which could be partially explained by the differences in the analyzed period and the use of different rainfall data sets.

Actual evapotranspiration estimated by GLEAM shows lower seasonality than rainfall and runoff (red line in Fig. 2), with maximum (minimum) values during December-March (June-August), corresponding to 3.9 mm/day and 2.0 mm/day, respectively. The seasonal cycle coincides well with the estimation of Sun et al. (2019) who used a water-budget approach for the whole Madeira Basin. In particular a distinctive characteristic present in both Sun et al. (2019) and GLEAMa data is that the annual cycle has its minimum value in June, which is a dry month. This is a feature that has been observed in recent studies and can probably be explained by plant phenology (e.g. Wu et al., 2016), commonly not present in land surface model-based E estimates (e.g. Sörensson and Ruscica, 2018). The mean actual evapotranspiration for the 1982–2017 period estimated over the upper Madeira Basin is 2.90 mm/day (Table 1). Lower annual values are observed over the Andean region (< 1.5 mm/day) and in the southernmost Madeira Basin (< 2 mm/day). In contrast, higher E estimations are observed over the Amazon-Andes transition region and in the northern part of the basin, where E is around 4 mm/day (not shown). This spatial pattern of E is coherent with previous studies that used several E data sources (e.g. Paca et al., 2019).

Based on these estimations, the surface water budget in the upper Madeira Basin (computed as P-R-E, using the long-term mean values of precipitation, runoff and evapotranspiration, respectively) is -0.34 mm/day, equivalent to -8% of the mean annual rainfall, which is close to balance within tolerance (< 10%) according to previous studies (e.g. Builes-Jaramillo and Poveda, 2017). Uncertainties in evapotranspiration are a possible source of this imbalance; however, recent studies have documented a rainfall underestimation in the interpolated and satellite-based rainfall estimations, particularly in the Amazon-Andes transition region, such as the upper Beni and the Madre de Dios river basins (Builes-Jaramillo and Poveda, 2018; Espinoza et al., 2015).

The monthly surface water budget (monthly P-E-R) and the monthly changes in terrestrial water storage (TWS) from the GRACE Mission (grey bars and dotted blue line in Fig. 2, respectively), are used as indicators of the state of the surface water, soil moisture and groundwater in the upper Madeira Basin during the hydrological year. Both data sources show positive (negative) values from October-March (April-September), which suggest that the soil is recharged with water during the August-February season, while during March to June the water storage is depleted. It is important to note that TWS shows a higher seasonality comparing to the monthly surface water budget, which is partially explained by the shorter TWS period (2002–2017), where several extreme floods (e.g. 2014; 2015) and droughts (e.g. 2005, 2010, 2016) have been reported in the upper Madeira Basin. Indeed, a better match between the monthly surface water budget and TWS is obtained when values for the common 2002–2017 period are computed (not shown). In particular, the monthly surface water budget for the 2002–2017 period shows higher values during the December-February wet season, reaching 2.7 mm/day in February (instead of 2.0 mm/day) and 2.3 mm/day in December (instead of 1.9 mm/day).

5. Interannual evolution of the runoff-rainfall relationship

As described above, Fig. 2 shows a lag of around two months between runoff and rainfall annual cycles. In order to estimate the characteristic rainfall-runoff time-lag (CT) at a basin scale over the upper Madeira, we compute a lagged correlation between daily rainfall and runoff (Fig. 3a). CT is computed using both CHIRPS and HOP spatially averaged daily rainfall products (see Section 3). The maximum coefficient of correlation between daily rainfall and runoff is obtained using 60-days lag for both products. Thus, Fig. 3a confirms that the mean CT for the upper Madeira Basin is around two months. In both cases (using CHIRPS and HOP), the evolution of r values shows similar shapes with a strong increase in the first 10 days of runoff lag (from 0.25 to 0.40; Fig. 3a). Based

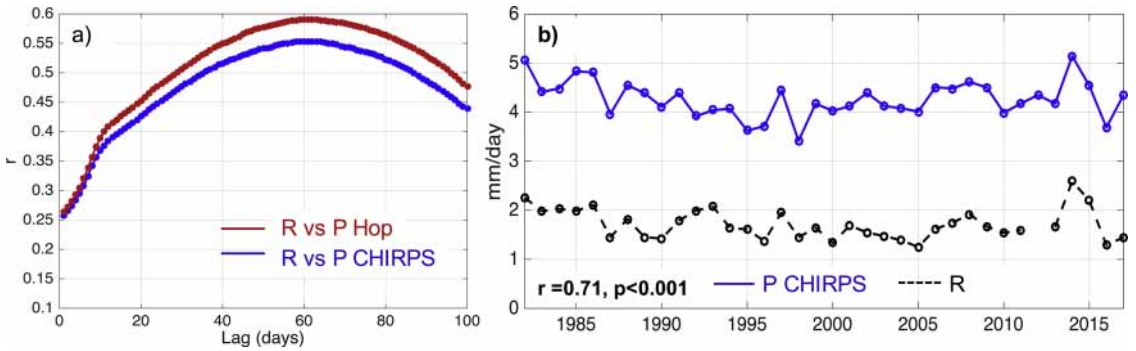

Fig. 3. a) Correlations between daily values of spatially averaged rainfall over the upper Madeira Basin and lagged observed runoff at Porto Velho station. Two rainfall data sets are used: HOP (1982–2009, red line) and CHIRPS (1982–2017, blue line). Lag is computed from zero (no lag) to 100 days. b) Interannual evolution of mean annual rainfall spatially averaged over the upper Madeira Basin (CHIRPS, blue line) considering the September-August hydrological year and runoff at Porto Velho station (black line) considering the November-October hydrological year (2011 is not taken into account due to missing runoff values). r and p values resulting from correlation between rainfall and runoff are indicated.

on the 60 days of CT and on the onset of the wet season in September that defines the beginning of the hydrological year (Fig. 2), the September-to-August (November-to-October) annual averages of P (R) is analyzed (Fig. 3b). In addition, when a seasonal analysis is conducted, September-to-November (November-to-January) is used to define the onset of the SAMS season and June-to-August (August-to-October) is used to define the dry season for rainfall (runoff).

The coefficient of correlation, r(P,R), between the mean annual runoff and rainfall is 0.71 (Fig. 3b and Table 1), which varies from 0.45 during the dry season to 0.73 during the onset of the SAMS (Table 1). These correlations are significant at $p < 0.001$. At annual time scale, no significant trend is detected in either rainfall or runoff over the upper Madeira. However, a significant diminution of evapotranspiration, (τ(E)), is identified ($p < 0.001$) with a break point in 1995 ($p < 0.05$) and lower values afterwards (Table 1). Nevertheless, in terms of absolute values, the detected E diminution plays a minor role in the basin water balance. Indeed, the 1982–2017 standard deviation of E is lower (0.07 mm/day) than the standard deviations of rainfall (0.38 mm/day) and runoff (0.31 mm/day) and E diminishes from 2.93 mm/day during the 1980s to 2.88 mm/day during the 21st Century, which corresponds to

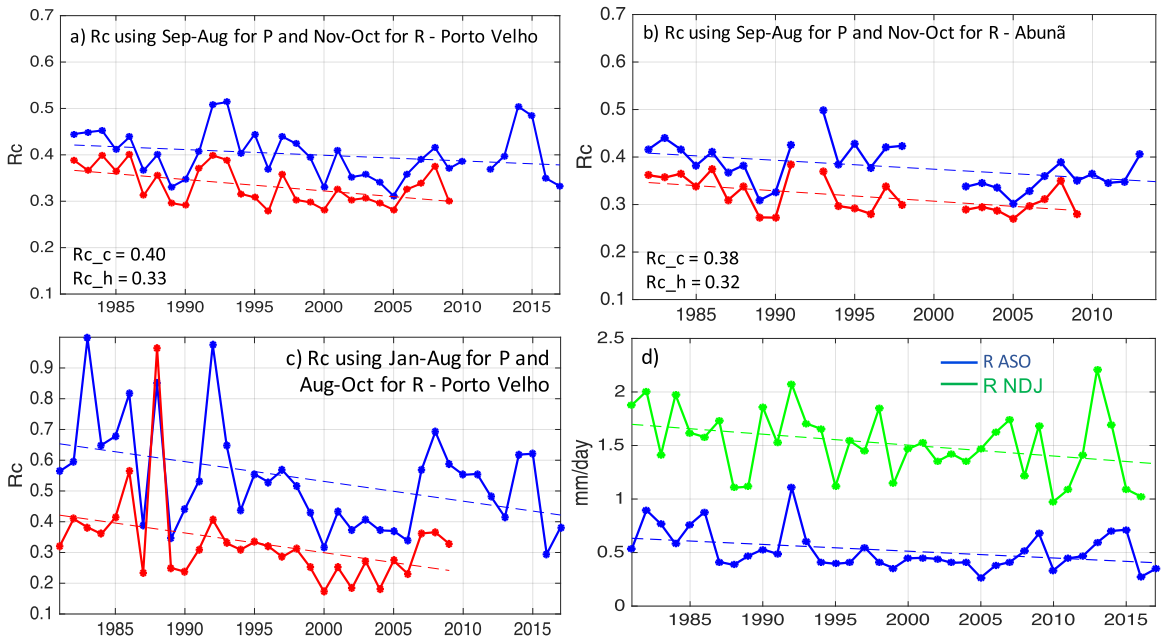

Fig. 4. Temporal evolution of the annual runoff coefficient (Rc = R/P) computed at (a) Porto Velho and (b) Abunã stations using HOP (Rc_h, red line, 1982–2009) and CHIRPS (Rc_c, blue line, 1982–2017) rainfall data. Annual cycle is computed from September-August and November-October for rainfall (P) and runoff (R), respectively. 1982–2017 mean annual Rc values for Porto Velho and Abunã basins are indicated in a and b, respectively. In Porto Velho (Abunã) 2011 (1992, 1999–2001 and 2017) are not taken into account due to missing runoff values. c) As (a), but Rc computed for the low-water period for August-October runoff and June-August rainfall. d) Interannual evolution of runoff at Porto Velho during November-January season (green line, 1981–2016) and during August-October season (blue line, 1981–2017). Trend lines are shown when significant ($p < 0.05$) according to Kendall coefficient.

2% of mean annual P.

In order to evaluate changes in the runoff-rainfall relationship over the upper Madeira Basin, the interannual evolution of Rc is estimated using CHIRPS and HOP rainfall data sets averaged over the Porto Velho and Abunã basins and runoff estimated at the same two stations (Figs. 4a and 4b, respectively). In all the cases a significant diminution of Rc is detected for the 1982–2017 period ($p < 0.05$), which cannot be directly explained by the significant diminution of actual evapotranspiration. Indeed, diminution trend in Rc is usually associated with an increase of water losses in the annual budget, such as increases of evapotranspiration. Considering a seasonal analysis of Rc, a significant diminution ($p < 0.05$) is only observed during the dry season (Fig. 4c) and significant diminution of evapotranspiration is only observed during December-February season (Table 1). Break points are detected in Rc at annual time scale and during the dry season in 1998 and 1997, respectively ($p < 0.05$) and lower values are observed afterwards. On the other hand, evapotranspiration shows break points in 1997 ($p < 0.01$) and 1995 ($p < 0.05$) during the December-February and March-May seasons, respectively.

Table 1 also shows that the interannual variability of Rc is particularly modulated by the interannual variability of runoff but not by rainfall interannual variability since the coefficient of correlation between runoff and Rc, r(R,Rc), is significant at $p < 0.01$ regardless of the season, while no significant correlation is observed between the interannual variability of rainfall and Rc, r(P,Rc). In coherence with these results, and in accordance with previous studies (Espinoza et al., 2009b; Molina-Carpio et al., 2017a), a significant runoff diminution is observed during the low-water season (August-to-October and November-to-January; $p < 0.05$, Fig. 4d) and a break point is identified in 1993 in August-to-October runoff ($p < 0.01$), with lower values afterwards (Table 1). These results suggest a change in the runoff-rainfall relationship in the upper Madeira Basin characterized by a runoff diminution during the low-water season that is not observed in the basin averaged rainfall, producing a significant diminution of the Rc. Nevertheless, evapotranspiration shows a significant diminution (particularly during the December-to-February wet season), which seems contradictory with the Rc diminution in the upper Madeira. These results suggest that changes in land-surface processes or changes in regional rainfall intensity may impact the observed Rc evolution. In the following section the regional influence of rainfall on runoff variability at Porto Velho is analyzed in order to better understand the observed changes in the rainfall-runoff relationship.

6. Regional rainfall influence on runoff at Porto Velho Basin

6.1. Regional change in the characteristic rainfall-runoff time-lag (CT) and seasonal rainfall-runoff relationship

Considering the large extension of the upper Madeira Basin (975,500 km^2) and the geomorphological and climatic diversity that characterize the basin, it is particularly important to analyze the regional rainfall influence on runoff variability. Computing the regional distribution of the CT over the basin (Fig. 5a) provides an initial overview. In this case, CT is computed using the significant coefficient of correlation between each the daily rainfall at grid point and the lagged daily runoff at Porto Velho (see Section 3). While the mean CT over the basin is estimated to 60 days (Fig. 3a), CT over the southern part of the basin (particularly south of 14 °S) is higher than the mean CT, reaching 65–75 days (Fig. 5a). In particular, high CT values are observed over the middle and upper Mamoré and Guaporé basins, upstream of the Llanos de Mojos floodplain. Indeed, a rapid transition in CT is identified above the 150 masl (grey line in Fig. 5a), which correspond to the mean elevation of the Llanos de Mojos floodplain (Guyot, 1993). Thus, Fig. 5a suggests that the Llanos de Mojos plays a relevant role in modulating the spatial distribution of CT over the upper Madeira Basin. Fig. 5a also displays low CT values over the Amazon-Andes transition region of the Madre de Dios and Beni rivers. These regions are characterized by extreme rainfall values and the presence of steep slopes (Fig. 1), which can explain lower CT values of 50–55 days.

In order to clarify the spatial distribution of CT over the Madeira Basin, Figs. 5b and 5c, show the variations of geomorphological parameters (altitude and slope) in relation to CT values along the first 1600 km of the river upstream of Porto Velho station, following the Guaporé and Beni tributaries. For this, distances vs. CT pairs are computed from Fig. 5a each 50 km; then, for each CT (at one day of resolution) we calculate the mean distance for all the pairs (black circles in Fig. 5b and 5c). Regarding the Guaporé River, the mean slope becomes near zero between 400 km and 1050 km from Porto Velho, at around 150 masl, which corresponds to the Llanos de Mojos floodplain. Downstream of the floodplain (between zero and 400 km from Porto Velho) CT is around 55 days, but this value increases over the floodplain region to 65 days. Finally, high CT values (65–75 days) are observed upstream of the floodplain (Fig. 5b). The extension of the floodplain along the Beni River is smaller comparing to Guaporé River. Minimal slope is identified between 250 km to 600 km from Porto Velho and CT over this region is around 60 days (Fig. 5c). About 1100 km from Porto Velho the slope of the Beni river increases, and the mean river altitude change from 200 masl to 300 masl. This region corresponds to the beginning of the rainfall hotspot region and lower CT values are found (45–55 days). The influence of the floodplain and the extreme rainfall zones (hotspot) are also remarkable in the Mamoré and Madre de Dios rivers (supplementary Figure S1).

These results provide new information regarding the spatial distribution of CT over the upper Madeira Basin and suggest a differentiated regional influence of rainfall on runoff at Porto Velho. Indeed, rainfall over the hotspot regions show a rapid influence on runoff (CT around 45–55 days) and rainfall over the southern part of the basin (particularly south of the 14 °S, upstream of the Llanos de Mojos floodplain), shows a delayed influence on runoff (CT around 75 days).

According to the above described results, we analyze the annual and seasonal correlation between rainfall in each grid point and runoff at Porto Velho (Fig. 6). At annual scale, rainfall over the middle Madre de Dios, Beni and Mamoré basins, which correspond to the rainiest regions of the basins, show a stronger influence on runoff variability (Fig. 6a). However, rainfall over the southern part of the basin shows low or no significant correlation with runoff at Porto Velho. This behavior is mostly related to the wet season pattern (Fig. 6c), with higher correlation values over the middle Beni Basin. During March-to-May (Fig. 6d), rainfall over the lowland is highly correlated to May-to-July runoff. Significant values also appear over the southeastern part of the basin (Mamoré and Guaporé

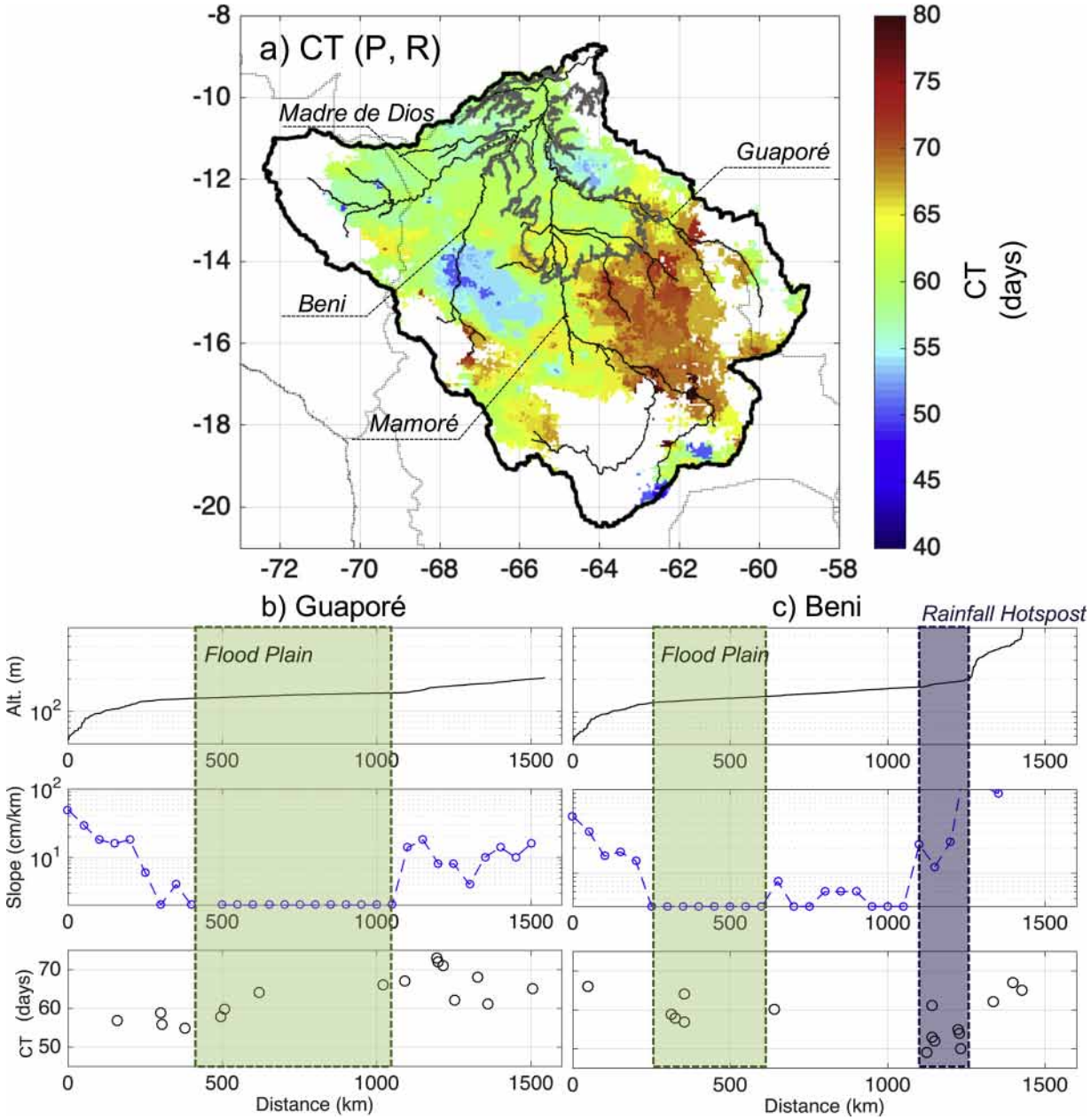

Fig. 5. a) Spatial distribution of the averaged 1981–2017 characteristic rainfall-runoff time-lag (CT, in days), computed between rainfall in each CHIRPS grid point (0.05°x0.05°) and daily runoff at Porto Velho station. Only significant correlated values ($p < 0.05$) between each CHIRPS rainfall grid and runoff at Porto Velho at annual scale are plotted (see Fig. 6a). The contour line of 150 masl is shown in dark gray color, corresponding to the mean altitude of the Llanos de Mojos flood plain (Guyot, 1993). Main rivers and topography were computed using Shuttle Radar Topography Mission (SRTM) at 90 m of resolution. b) and c) show the altitude, mean river slope and mean CT in the top, middle and bottom panels, respectively, of two main tributaries: Guaporé and Beni following the river upstream from Porto Velho. Only the first 1600 km of river upstream from Porto Velho are plotted. Note that y axes of altitude and slope are displayed in a logarithmic scale. The location of the Beni and Guaporé rivers is indicated in panel (a). The slope is computed as the difference of river altitude each 50 km. From panel (a) *distances vs. CT* pairs are computed; then, for each CT (at one day of resolution) we calculate the mean distance for all the pairs (black circles in b and c). In (b) and (c) the green regions represent the zone with minimal slope, associated to the Llanos de Mojos flood plain, while the blue region in (c) represents the position of the "rainfall hotspot" region in the upper Beni River.

basins) and no significant correlation is observed over the Andean region (Fig. 6d). During the dry season and the beginning of the hydrological year, rainfall over the southern part of the basin is significantly correlated to runoff, particularly over the upper Beni, Mamoré and Guaporé basins, and in the upper Madre de Dios during September-November season (Fig. 6e and 6b). These results show that runoff during the high-water period (February-to-April) is more dependent on rainfall over the northwestern part of the

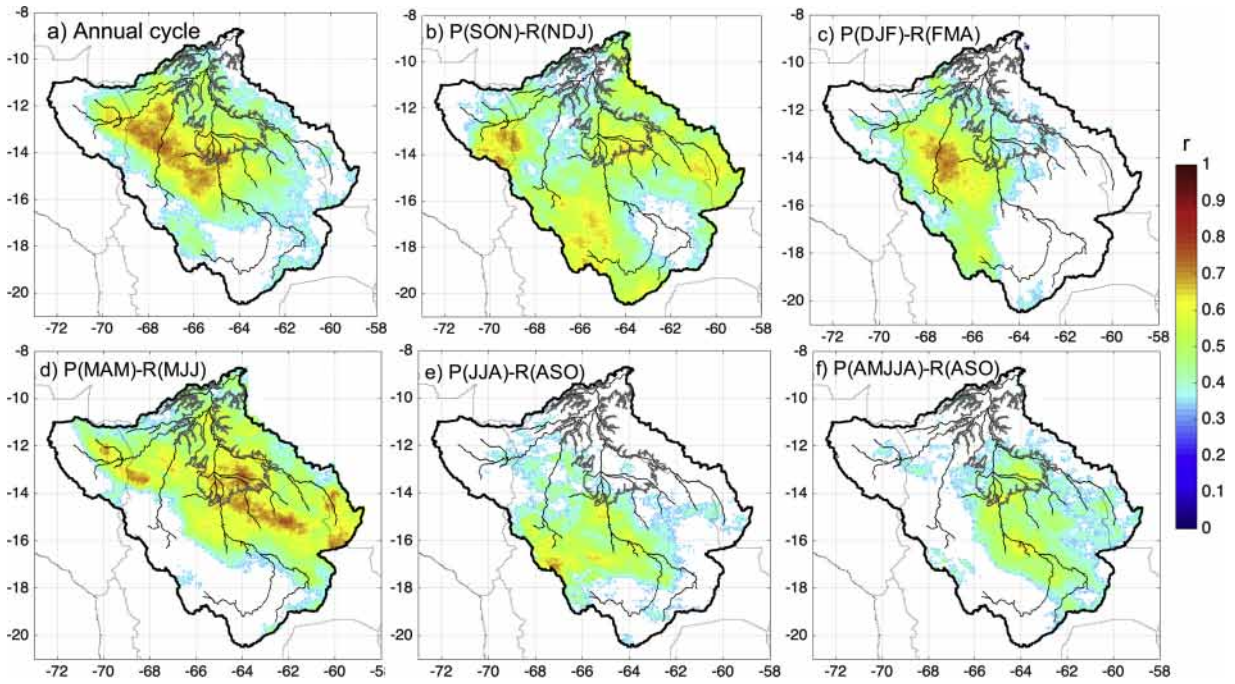

Fig. 6. 1982–2017 rainfall-runoff correlation in the upper Madeira Basin computed between each CHIRPS rainfall grid and runoff at Porto Velho. Only significant values at $p < 0.05$ are plotted. In a) the annual cycle is defined as September-August for rainfall and November-October for runoff. In b) to e) the three-monthly correlation is computed for September-November and November-January (for rainfall and runoff, respectively) to June-August and August-October (for rainfall and runoff, respectively). In f) rainfall over the April-August season is correlated to runoff during the low-water season (August-October). Note that in panels (a) and (c) correlation were computed for the 1982–2017 period and the year 2011 is not taken into account due to missing runoff values. Contour line of 150 masl and main rivers are shown in dark gray and black colors, respectively.

basin, particularly over Beni and Madre de Dios basins, and during the low-water season (August-to-October) runoff is more related to rainfall over the southern part of the basin. However, the southern part of the basin shows higher CT values (~75 days, Fig. 5a), suggesting a slow influence of rainfall over this region on runoff at Porto Velho, probably associated with the role of the Llanos de Mojos floodplain (Fig. 5a and 5b). Therefore, we compute the correlation between spatialized rainfall during a larger season, from April-to-August, and runoff during the low-water period (August-to-October) at Porto Velho (Fig. 6f). The results confirm that rainfall over the southern part of the basin upstream of the Llanos de Mojos floodplain is significantly correlated to runoff at Porto Velho during the low-water period. In addition, during the dry season (June-to-August) rainfall in the south of 14 °S represent 44% of the mean rainfall over the upper Madeira Basin. These results suggest that not only the evolution of the basin areal mean rainfall is important to understand runoff evolution at Porto Velho, but that the analysis on a sub basin scale is also necessary.

6.2. Changes in regional rainfall patterns

In a recent study, Espinoza et al. (2019) show an increase of the dry day frequency (DDF, defined as the number of days with rainfall < 1 mm) over the southern Amazon Basin, particularly during the transitional September-November season. In addition, the authors documented a diminution in the frequency of wet days (WDF, defined as the number of days with rainfall > 10 mm) during this season. In Fig. 7 we provide a more detailed analysis of the seasonal 1981–2017 evolution of the DDF and WDF over the upper Madeira Basin using CHIRPS rainfall data. Over the southern part of the basin, particularly south of 14 °S, a significant diminution of WDF and an increase of DDF are observed, suggesting drier conditions over this region. This pattern is observed in all the seasons with some specificities. For instance, diminution of WDF is remarkable along the year (with more intensity during September-to-November and March-to-May; Fig. 7a and 7e) and the increase of DDF is more intense during September-to-November and December-to-February over the southern upper Madeira Basin (Fig. 7b, d and f). These changes do not occur over the Andean Beni River Basin at Rurrenabaque station, where no decreasing runoff trends were observed (Molina-Carpio et al., 2017). Moreover, during the wet December-to-February season WDF significantly increase over the northern part of the basin, particularly to the north of 14 °S (Fig. 7c). These results confirm a contrasted evolution of rainfall intensity in the upper Madeira Basin, characterized by increasing WDF in the north (particularly during the wet season) and decreasing WDF and increasing DDF in the south during the entire hydrological year.

The regional evolution of total rainfall at annual and seasonal time scales is provided in Figs. 8 and 9, considering two regions: the southern part of the basin (south of the 14 °S, in red) and the northern part (north of the 14 °S, in blue). These two regions are chosen due to the observed changes in rainfall intensity (WDF and DDF, Fig. 7) and based on the differences of the regional CT observed in

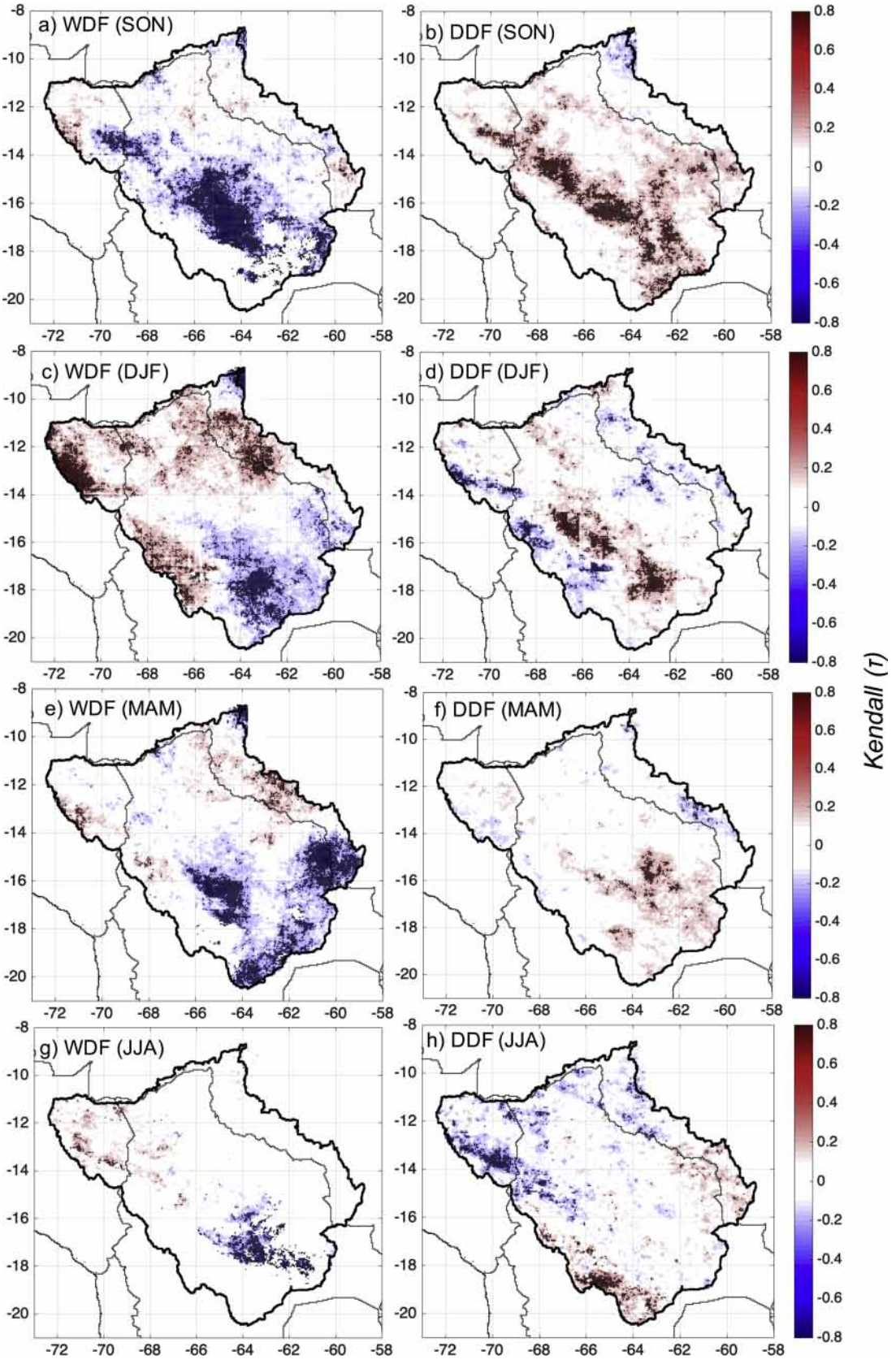

(caption on next page)

Fig. 7. Spatial distribution of Kendall coefficient values ($p < 0.05$ are displayed with a dark dot) indicating the trend for 1981–2017 wet-day frequency (WDF, left panels) and dry-day frequency (DDF, right panels) computed in each CHIRPS rainfall grid (0.05°x0.05°) over the upper Madeira Basin during a), b) September–November, c), d) December–February, e), f) March–May, and g), h) June–August seasons. In panels (c) and (d) the trend analysis are computed for the 1982–2017 period.

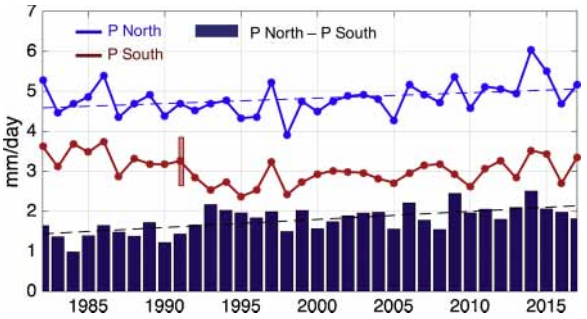

Fig. 8. 1982–2017 interannual rainfall evolution spatially averaged over the southern (South of 14 °S, red line) and northern (North of 14 °S, blue line) upper Madeira Basin. Annual rainfall regime is computed from September (year n-1) to August (year n). Temporal evolution of the differences between rainfall in northern and southern upper Madeira is indicated by blue bars. Trend lines are shown when significant ($p < 0.05$) according to Kendall coefficient. Red bar means a break point ($p < 0.05$) in southern annual rainfall identified in 1991, based on Pettitt test.

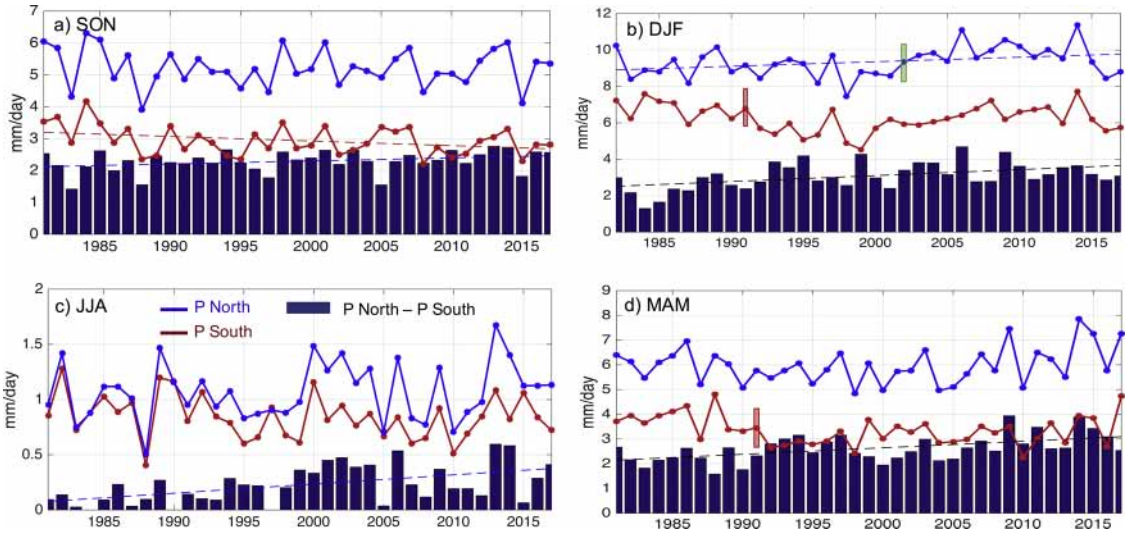

Fig. 9. As Fig. 8 but for a three-monthly analysis: a) September-November, b) December-February, c) June-August and d) March-May. Red bar means a break point in southern rainfall identified in December-February of 1991 and March-May of 1992, while green bar means a break point in northern rainfall identified in December-February of 2002. Red (green) bar means a rainfall diminution (increasing) after the break date. All break points are based on Pettitt test at $p < 0.05$.

Table 2
As Table 1, but considering rainfall and evapotranspiration in southern (South of 14 °S, denoted as PS and ES, respectively) and northern (North of 14 °S, denoted as PN and EN) upper Madeira basin. Trends and breaks analyses are also provided for the annual differences between rainfall in the northern upper Madeira Basin minus rainfall in the southern Madeira Basin (PN-PS). Only values with $p < 0.1$ are indicated in correlation, trend and break analysis. Values significant at $p < 0.05$ ($p < 0.01$) are underlined and in italic (bold). Years in red (blue) color means that a diminution (increasing) is reported after the break point.

	PS(mm/d)	PN(mm/d)	r(PS,R)	r(PN,R)	τ(PS)	τ(PN)	τ(PN-PS)	τ(ES)	τ(EN)	Pett(PS)	Pett(PN)	Pett(PN-PS)	Pett(ES)	Pett(EN)
Mean Annual	3.03	4.82	**0.60**	**0.60**	---	*0.27*	**0.45**	**-0.38**	---	***1991***	---	1991	***1995***	---
Sept-Nov (Nov-Jan)	2.94	5.23	**0.73**	**0.69**	*-0.21*		*0.23*	---	---	---	---	---	---	---
Dec-Feb (Feb-Apr)	6.26	9.34	**0.53**	**0.47**	---	*0.22*	**0.33**	**-0.52**	**-0.32**	*1991*	*2002*	1992	***1997***	*2007*
Mar-May (May-Jul)	3.36	5.98	**0.58**	**0.64**	---	---	**0.34**	*-0.28*	---	***1992***	---	*2005*	*1995*	---
Jun-Aug (Aug-Oct)	0.84	1.07	**0.52**	---	---	---	**0.36**	---	**0.30**	---	---	1997	---	*1999*

Fig. 5a and the seasonal rainfall influence on the runoff at Porto Velho (Section 6.1; Fig. 6). At the annual scale (September-August), rainfall in the northern part of the basin shows a significant increase ($p < 0.05$) and no break points are detected (Table 2). Over the southern part of the basin no trend is observed in annual rainfall, however rainfall in the south shows a shift in 1991 ($p < 0.05$) with lower values after this date (Table 2). As a consequence, the annual difference between rainfall over the northern and southern part of the basin (blue bars in Fig. 8) significantly increase ($p < 0.01$) and a shift is detected in 1991 ($p < 0.01$), with larger differences after this date (Table 2). At the annual scale, actual evapotranspiration diminishes in the southern part of the basin (Table 2, $p < 0.01$) and a shift is detected in 1995 ($p < 0.01$), four years after the shift observed in rainfall in the south. However, over the northern part of the basin, no evapotranspiration trend or shift is detected.

At the seasonal scale (Fig. 9), diminution in rainfall over the southern basin is remarkable during September-November (Fig. 9a), where a negative rainfall trend in the south is detected ($p < 0.1$) and a shift is observed in 1991 (1992) during December-February (March-May), significant at $p < 0.1$ ($p < 0.05$). Dryer conditions are observed after this date (Fig. 9b and d; Table 2). These results suggest that runoff diminution observed in Porto Velho during the low-water season is associated with drier condition over the southern part of the basin. In particular, both the low-water time series of runoff and rainfall in the south are characterized by shifts at the beginning of the 1990s (Tables 1 and 2), with lower values afterwards. Indeed, the shifts detected in low-water runoff in 1993 can be associated with the shift detected in rainfall over the southern part of the basin in 1991-92. As documented in Section 6.1 and Fig. 6, rainfall over the southern part of the basin plays a key role to modulate runoff variability at Porto Velho during the low-water period. Analyzing the coefficient of correlation between rainfall in the northern and southern part of the basin vs. runoff at Porto Velho, Table 2 shows that seasonal rainfall over both regions are significantly correlated with seasonal runoff, except for runoff during the low-water season. During this season runoff is only significantly correlated to rainfall in the south, which is in accordance with Fig. 6f.

Regarding rainfall in the northern part of the basin, a positive trend is detected in December-February ($p < 0.1$) and a break point is observed in 2002 ($p < 0.05$). Increase in northern basin December-to-February rainfall is coherent with the WDF intensification in this region (Fig. 7c), which translate in a rainfall increase in the north at the annual scale (Fig. 8). Fig. 9 and Table 2 also document a significant increase of the regional rainfall differences at annual and seasonal scales over the 1983–2017 period. Difference increase is significant at $p < 0.01$, except for the September-to-November season that is significant at $p < 0.05$ (Fig. 9, Table 2). Evapotranspiration in the south significantly diminishes during December-to-February and March-to-May ($p < 0.01$ and $p < 0.05$, respectively) and shifts are observed in 1997 and 1995, respectively, with lower values after these dates (Table 2). That is, a few years later than the shift of rainfall in the south (1991–1992). Finally, evapotranspiration in the north shows a diminution trend during December-to-February ($p < 0.01$), a downward shift in 2007 ($p < 0.05$) and an increasing trend during June-to-August ($p < 0.01$; Table 2).

These results provide new information regarding the spatial rainfall evolution over the upper Madeira Basin, which is a key issue to clarify the reason of the observed changes in the hydrological regime at a basin scale. Indeed, the Rc diminution reported in Section 5 (Fig. 4a) is particularly associated with the runoff diminution during the low-water season (Fig. 4d and Table 1) and with the diminution in rainfall over the southern part of the basin, particularly after 1991-92. However, during the wet season, total rainfall and WDF significantly increase over the northern part of the basin, an increase that also is perceptible at the annual scale. The increase in precipitation in the north and the decrease in the south are compensated at the basin scale, where no trend is detected in annual rainfall and runoff. However, this contrasted rainfall evolution has significantly impacted the rainfall seasonality over the basin and the evolution of Rc.

In addition, associated with rainfall diminution and DDF increase in the southern part of the basin, a significant diminution in evapotranspiration has been detected over this region. While annual rainfall in the south shifted in 1991 and drier conditions are observed after this date, annual evapotranspiration in the south shifted in 1995 and lower values are observed after this date. Diminution in actual evapotranspiration in the southern Madeira can be related to a diminution in rainfall over this region and/or a reduction of the tropical forest, as documented in previous studies (see Introduction).

7. Conclusions and final comments

During the last four decades scientific literature has documented climatic and environmental changes in southern Amazonia, including the upper Madeira Basin (975,500 km^2). In this study, we document that the runoff coefficient (Rc: runoff/rainfall) in the upper Madeira Basin, an indicator of environmental changes over the basin, decreases during the 1982–2017 period and in particular during the dry season. Rc diminution is associated with a significant runoff diminution ($p < 0.05$) during the low-water season (August-to-October). However, in terms of basin-averaged rainfall, no trend is detected. Therefore, an analysis at the basin scale is not satisfactory to explain the changes observed in Rc and is a first argument for developing an analysis at the sub-regional level.

Initially, we provide a comprehensive analysis of the surface water budget over the basin using i) daily runoff (R) at Porto Velho and Abunã stations, ii) daily rainfall (P), iii) evapotranspiration (E) and iv) terrestrial water storage (TWS). The surface water balance for the 1982–2017 period shows an imbalance of -0.34 mm/day, equivalent to -8% of the mean annual P, which is acceptable according to previous studies over the Amazon basin. The mean characteristic rainfall-runoff time-lag (CT) into the basin, which is an indicator of the mean travel time of the streamflow wave through the catchment, is estimated to 60 days, considering the basin-averaged P and R in Porto Velho. However, CT is higher (65–75 days) in the southern part of the basin, upstream of the Llanos de Mojos floodplain, and lower (50 days) over the Amazon-Andes transition regions (characterized by extreme rainfall values and high slopes). These results confirm that a regional rainfall analysis is required in order to understand runoff variability and change at a basin scale. It is important to notice that in this study, CT is estimated using a statistical approach (i.e. rainfall-runoff correlations)

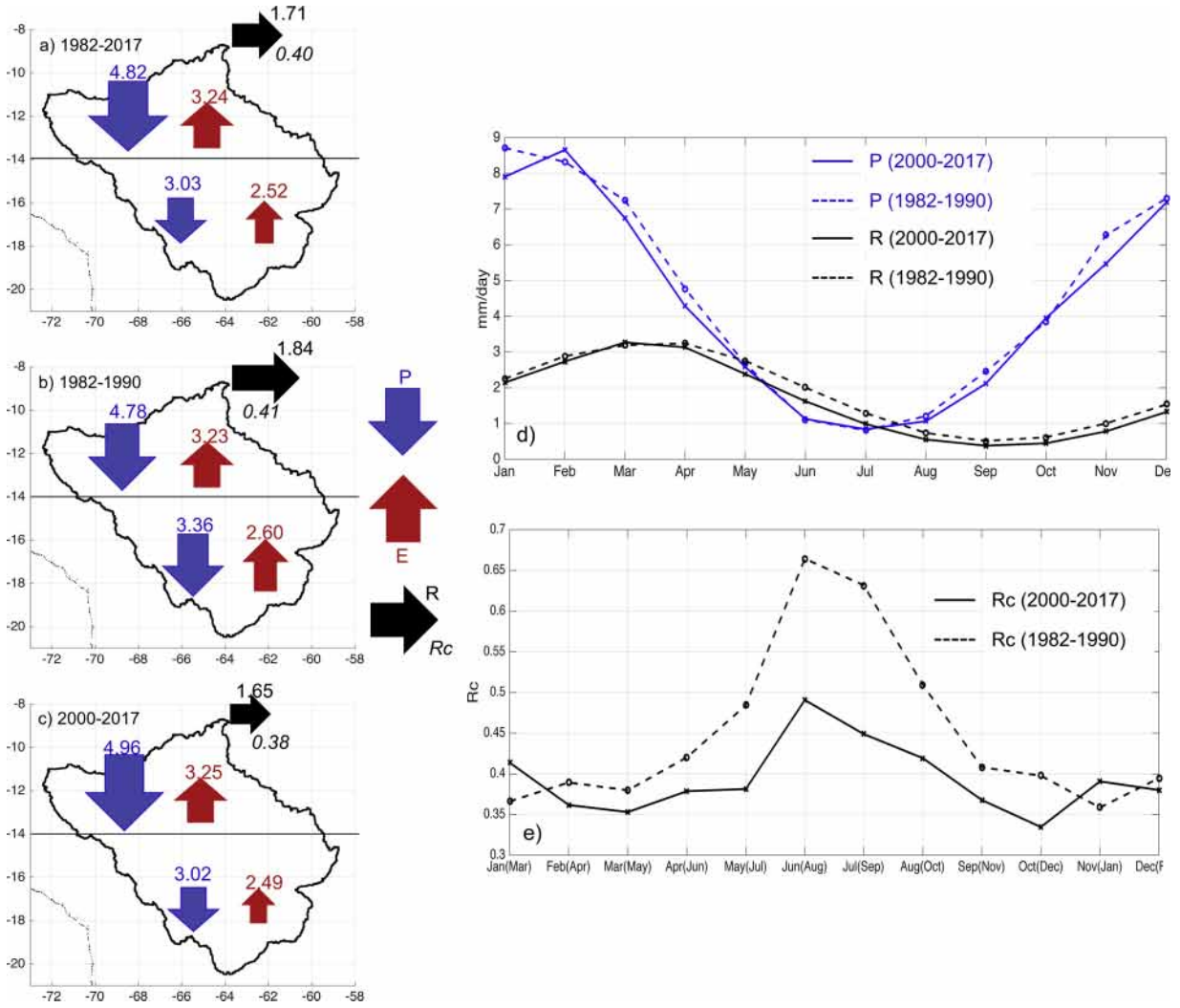

Fig. 10. a) – c) Schematic illustration of the regional water balance for three different periods. Rainfall (P, in blue, estimated using CHIRPS) and evapotranspiration (E, in red) in the northern and southern upper Madeira Basin, runoff (R, in black) and runoff coefficient (Rc, in black) at Porto Velho station during: a) 1982–2017, b) 1982–1990 and c) 2000–2017 periods. Values are in mm/day with exception of Rc (dimensionless). d) Annual cycle of rainfall (blue lines) and runoff (black lines) over the whole upper Madeira Basin during the 1982–1990 period (dotted lines) and during 2000–2017 period (solid lines). e) As d) but for monthly runoff coefficient (Rc). In the X axe the months without parenthesis (between parentheses) corresponds to rainfall (runoff).

and for a better understanding of the influence of the geomorphological and climatic features on CT, physical-based methods would be required.

Fig. 10 and Table 2 summarize regional P and E at annual and seasonal time scales, considering the whole study period and two sub periods (1982–1990 and 2000–2017) as well as runoff and runoff coefficient at Porto Velho station. These sub periods are chosen because temporal shifts in P, R, E and Rc are detected during the 1990s (Table 2). Over the northern part of the basin (north of 14 °S), P and the frequency of wet days ($P > 10$ mm/day) significantly increase, particularly during the wet season, while E remains constant at annual scale. Over the southern part of the basin (south of 14 °S) dry conditions are intensified, characterized by an increase in the frequency of dry days ($P < 1$ mm/day) and a diminution in the mean annual P after 1991 ($p < 0.05$). In addition, a shift is detected in P time series during December-February and March-May over the southern part of the basin in 1991 and 1992, respectively ($p < 0.05$) with drier conditions afterward, which contributes to explain a shift detected in R during the low-water season in 1993 ($p < 0.01$). E also diminishes significantly over the southern part of the basin at annual scale ($p < 0.01$) and a shift is detected in 1995 with lower values after this date. During the 21st Century, annual P in the south is even lower than E in the northern part of the basin (Fig. 10c). Drier conditions in the southern Madeira Basin could affect negatively vegetation conditions and agriculture activities, and therefore the economy of the driving Santa Cruz region in Bolivia. The regional changes documented in this study have modified the hydrological annual cycle of the upper Madeira Basin during the last two decades (Fig. 10d). During the recent period lower rainfall (runoff) are observed from March to November (May to February), and no change is observed during the

wet period, except for a rainfall (runoff) increase in February (March). As a consequence, Rc significantly decreases during the dry season (from 0.60 to 0.45 in average), but no significant changes are observed during the wet season (around 0.40; Fig. 10 e).

The contrasting evolution of rainfall between the north (increase) and south (decrease) has a significant impact on the Rc evolution of the upper Madeira Basin during the 1982–2017 period. In addition, our results suggest changes in the atmosphere and land surface interactions over the southern part of the Madeira Basin since the beginning of the 1990. P diminution in the southern Madeira Basin is in accord with the lengthening of the dry season reported in previous studies in southern Amazonia, which has been related to an increase of atmospheric subsidence (e.g. Yoon and Zeng, 2010; Agudelo et al., 2018; Espinoza et al., 2019). E diminution in the southern Madeira is probably associated with a diminution in rainfall over this region and/or a reduction of the tropical forest. However, explanations for the decrease in E over this region need to be addressed in further studies.

Acknowledgments

This research has been supported by the French AMANECER-MOPGA project funded by ANR and IRD (ref. ANR-18-MPGA-0008). A. Sörensson and R. Ruscica acknowledge support from Belmont Forum/ANR-15-JCL/-0002-01 “CLIMAX”, PICT 2014-0887 and PICT-2015-3097 (ANPCyT, Argentina). The authors are grateful to the SNO-HYBAM observatory for providing rainfall and runoff data (available at: http://www.ore-hybam.org). We wish to thank the following agencies/organizations for providing access to data: The Climate Hazards Group Infrared Precipitation for providing CHIRPS data (information available at http://chg.geog.ucsb.edu/data/chirps/), Ghent University for providing GLEAM data (https://www.gleam.eu/), the Jet Propulsion Laboratory (JPL), the University of Texas Center for Space Research (CSR) and the Geo Forschungs Zentrum (GFZ) Potsdam for provide GRACE data (data are available at https://podaac.jpl.nasa.gov/dataset/TELLUS_LAND_NC_RL05) and Shuttle Radar Topography Mission (SRTM-V4.1) for providing DEM data (available at http://srtm.csi.cgiar.org/srtmdata/).

Appendix A. Supplementary data

Supplementary material related to this article can be found, in the online version, at doi:https://doi.org/10.1016/j.ejrh.2019.100637.

References

Agudelo, J., Arias, P.A., Vieira, S.C., Martínez, J.A., 2018. Influence of longer dry seasons in the Southern Amazon on patterns of water vapor transport over northern South America and the Caribbean. Clim. Dyn. https://doi.org/10.1007/s00382-018-4285-1.

Arias, P.A., Fu, R., Vera, C., Rojas, M., 2015. A correlated shortening of the North and South American monsoon seasons in the past few decades. Clim. Dyn. https://doi.org/10.1007/s0038. 2-015-2533-1.

Azarderakhsh, M., Rossow, W.B., Papa, F., Norouzi, H., Khanbilvardi, R., 2011. Diagnosing water variations within the amazon basin using satellite data. J. Geophys. Res. Atmos. 116, 1–18. https://doi.org/10.1029/2011JD015997.

Barichivich, J., Gloor, E., Peylin, P., Brienen, R.J.W., Schönegart, J., Espinoza, J.C., Pattnayak, K.C., 2018. Recent intensification of amazon flooding extremes driven by strengthened walker circulation. Sci. Adv. 4. https://doi.org/10.1126/sciadv.aat8785.

Beck, H.E., van Dijk, A.I.J.M., Levizzani, V., Schellekens, J., Miralles, D.G., Martens, B., de Roo, A., 2017. MSWEP: 3-hourly 0.25_ global gridded precipitation (1979–2015) by merging gauge, satellite, and reanalysis data. Hydrol. Earth Syst. Sci. 21, 589–615. https://doi.org/10.5194/hess-21-589-2017.

Bookhagen, B., Strecker, M.R., 2008. Orographic barriers, high-resolution TRMM rainfall, and relief variations along the eastern Andes. Geophys. Res. Lett. 35, L06403. https://doi.org/10.1029/2007GL032011.

Boisier, J.P., Ciais, P., Ducharne, A., Guimberteau, M., 2015. Projected strengthening of Amazonian dry season by constrained climate model simulations. Nat. Clim. Change 5 (7), 656–660.

Bourrel, L., Phillips, L., Moreau, S., 2009. The dynamics of floods in the Bolivian Amazon basin. Hydrol. Processes 23, 3161–3167. https://doi.org/10.1002/hyp.v23:22.

Builes-Jaramillo, L.A., Poveda, G., 2018. Conjoint analysis of surface and atmospheric water balances in the Andes-Amazon system. Water Resour. Res. 54 (5), 3472–3489. https://doi.org/10.1029/2017WR021338.

Chen, J.L., Wilson, C.R., Tapley, D.B., 2010. The 2009 exceptional Amazon flood an interannual terrestrial water storage change observed by GRACE. Water Resour. Res. 46, W12526 https ://doi. org/10.1029/2010W R0093 83.

Christoffersen, B.O., Restrepo-Coupe, N., Altaf Arain, M., Baker, I.T., Cestaro, B.P., Ciais, P., Fisher, J.B., Galbraith, D., Guan, X., Gulden, L., van den Hurk, B., Ichii, K., Imbuzeiro, H., Jain, A., Levine, N., Miguez-Macho, G., Poulter, B., Roberti, D.R., Sakaguchi, K., Sahoo, A., Schaefer, K., Shi, M., Verbeeck, H., Yang, Z.-L., Araújo, A.C., Kruijt, B., Manzi, A.O., da Rocha, H.R., von Randow, C., Muza, M.N., Borak, J., Costa, M.H., Gonçalves de Gonçalves, L.G., Zeng, X., Saleska, S.R., 2014. Mechanisms of water supply and vegetation demand govern the seasonality and magnitude of evapotranspiration in Amazonia and Cerrado. Agric. For. Meteorol. 191 (15), 33–50.

Debortoli, N.S., Dubreuil, V., Funatsu, B., Delahaye, F., Henke de Oliveira, C., Rodrigues-Filho, S., Saito, H., Fetter, C.R., 2015. Rainfall patterns in the Southern Amazon: a chronological perspective (1971–2010). Clim. Change 132, 251–264. https://doi.org/10.1007/s1058. 4-015-1415-1.

Espinoza, J.C., Chavez, S., Ronchail, J., Junquas, C., Takahashi, K., Lavado, W., 2015. Rainfall hotspots over the southern tropical Andes: spatial distribution, rainfall intensity and relations with large-scale atmospheric circulation. Water Resour. Res 51. https://doi.org/10.1002/2014WR016273.

Espinoza, J.C., Marengo, J.A., Ronchail, J., Molina, J., Noriega, L., Guyot, J.L., 2014. The extreme 2014 flood in South-Western amazon basin: the role of tropical-subtropical South Atlantic SST gradi- ent. Environ. Res. Lett. 9, 124007. https://doi.org/10.1088/1748-9326/9/12/124007.

Espinoza, J.C., Ronchail, J., Guyot, J.L., Cocheneau, G., Filizola, N., Lavado, W., de Oliveira, E., Pombosa, R., Vauchel, P., 2009a. Spatio-temporal rainfall variability in the amazon Basin countries (Brazil, Peru, Bolivia, Colombia and Ecuador). Int. J. Climatol. 29, 1574–1594.

Espinoza, J.C., Guyot, J.L., Ronchail, J., Cochonneau, G., Filizola, N., Fraizy, P., Labat, D., de Oliveira, E., Julio Ordonez, J., Vauchel, P., 2009b. Contrasting regional discharge evolutions in the Amazon basin (1974–2004). J. Hydrol. 375 (3–4), 297–311.

Espinoza, J.C., Ronchail, J., Marengo, J.A., Segura, H., 2019. Contrasting North–South changes in Amazon wet-day and dry-day frequency and related atmospheric features (1981–2017). Clim. Dyn. https://doi.org/10.1007/s00382-018-4462-2.

Farr, T.G., Caro, E., Crippen, R., Duren, R., Hensley, S., Kobrick, M., Paller, M., Rodriguez, E., Rosen, P., Roth, L., Seal, D., Shaffer, S., Shimada, J., Umland, J., Werner, M., Burbank, D., Oskin, M., Alsdorf, D., 2007. The shuttle radar topography mission. Rev. Geophys. 45 (2).

Frappart, F., Papa, J., Santos da Silva, G., Ramillien, C., Prigent, F., Seyler, C.S., 2012. Surface freshwater storage and dynamics in the amazon basin during the 2005 exceptional drought. Environ. Res. Lett. 7, 044010. https://doi.org/10.1088/1748-9326/7/4/044010.

Frappart, F., Ramillien, G., Ronchail, J., 2013. Changes in terrestrial water storage versus rainfall and discharges in the Amazon basin. Int. J. Climatol. 33, 3029–3046. https://doi.org/10.1002/joc.3647.
Fu, R., Yin, L., Li, W., Arias, P.A., Dickinson, R.E., Huang, L., Fernandes, K., Liebmann, B., Fisher, R., Myneni, R.B., 2013. Increased dry-season length over southern Amazonia in recent decades and its impli- cation for future climate projection. Proc. Natl. Acad. Sci. U. S. A. 110, 18110–18115.
Funk, C., Peterson, P., Landsfeld, M., Pedreros, D., Verdin, J., Shukla, S., Husak, G., Rowland, J., Harrison, L., Hoell, A., Michaelsen, J., 2015. The climate hazards infrared precipitation with stations—a new environmental record for monitoring extremes. Sci. Data 2 (150066), 2015. https://doi.org/10.1038/sdata.2015.66.
Getirana, A.C.V., et al., 2011. Calibração e Validação de Modelo Hidrológico com Observaçoes In Situ, Altimetria e Gravimetria Espaciais. Rev. Bras. Recursos Hídricos 16 (1), 29–45.
Getirana, A.C.V., et al., 2014. Water balance in the Amazon basin from a land surface model ensemble. J. Hydrometeor. 15, 2586–2614.
Guimberteau, M., Drapeau, G., Ronchail, J., Sultan, B., Polcher, J., Martinez, J.-M., Prigent, C., Guyot, J.-L., Cochonneau, G., Espinoza, J.C., Filizola, N., Fraizy, P., Lavado, W., De Oliveira, E., Pombosa, R., Noriega, L., Vauchel, P., 2012. Discharge simulation in the sub-basins of the Amazon using ORCHIDEE forced by new datasets. Hydrol. Earth Syst. Sci. 16, 911–935. https://doi.org/10.5194/hess-16-911-2012.
Guimberteau, M., Ronchail, J., Espinoza, J.C., Lengaigne, M., Sultan, B., Polcher, J., Drapeau, G., Guyot, J.L., Ducharne, A., Cialis, P., 2013. Future changes in precipitation and impacts on extreme stream- flow over Amazonian sub-basins. Environ. Res. Lett. 8, 014035. https://doi.org/10.1088/1748-9326/8/1/014035.
Guyot, J.L., 1993. Hydrogéochimie des fleuves de l' Amazonie bolivienne. Thesis (PhD). Collection etudes & theses. ORSTOM.
Guyot, J.L., et al., 1996. Dissolved solids and suspended sediment yields in the Rio Madeira basin, from the Bolivian Andes to the Amazon. In: In: Walling, D.E. (Ed.), Erosion and Sediment Yield: Global and Regional Perspectives. Wallingford: International Association of Hydrological Sciences 236. IAHS Publication, pp. 55–63.
Hamilton, S.K., Sippel, S.J., Melack, J.M., 2004. Seasonal inundation patterns in two large savanna floodplains of South America: the Llanos de Moxos(Bolivia) and the llanos del Orinoco (Venezuela and Colombia). Hydrol. Processes 11, 2103–2116. https://doi.org/10.1002/hyp.5559.
Junquas, C., Takahashi, K., Condom, T., Espinoza, J.C., Chavez, S., Sicart, J.E., Lebel, T., 2018. Understanding the influence of orography over the precipitation diurnal cycle and the associated atmospheric processes in the central Andes. Clim. Dyn. https://doi.org/10.1007/s00382-017-3858-8.
Killeen, T.J., Douglas, M., Consiglio, T., Jørgensen, P.M., Mejia, J., 2007. Dry spots and wet spots in the Andean hotspot. J. Biogeogr. 34 (8), 1357–1373. https://doi.org/10.1111/j.1365–2699.2006.01682.x.
Kendall, M., 1975. Rank Correlation Methods. Grifin, London.
Liu, Y.Y., Dorigo, W.A., Parinussa, R.M., de Jeu, R.A.M., Wagner, W., McCabe, M.F., Evans, J.P., van Dijk, A.I.J.M., 2012. Trend-preserving blending of passive and active microwave soil moisture retrievals. Remote Sens. Environ. 123, 280–297. https://doi.org/10.1016/j.rse.2012.03.014.
Liu, Y.Y., van Dijk, A.I.J.M., McCabe, M.F., Evans, J.P., de Jeu, R.A.M., 2013. Global vegetation biomass change (1988–2008) and attribution to environmental and human drivers. Glob. Ecol. Biogeogr. 22, 692–705. https://doi.org/10.1111/geb.12024.
Lopes, A.V., et al., 2016. Trend and uncertainty in spatial- temporal patterns of hydrological droughts in the Amazon basin. Geophys. Res. Lett. 43 (7), 3307–3316. https://doi.org/10.1002/2016GL067738.
Maeda, E.E., Kim, H., Aragão, L.E.O.C., Famiglietti, J.S., Oki, T., 2015. Disruption of hydroecological equilibrium in southwest Amazon mediated by drought. Geophys. Res. Lett. https://doi.org/10.1002/2015GL065252.
Marengo, J.A., Espinoza, J.C., 2016. Review article. Extreme seasonal droughts and floods in Amazonia: causes, trends and impacts. Int. J. Climatol. https://doi.org/10.1002/joc.4420.
Marengo, J.A., Tomasella, J., Alves, L.M., Soares, W., Rodriguez, D.A., 2011. The drought of 2010 in the context of historical droughts in the Amazon region. Geophys. Res. Lett. 38, 1–5.
Marengo, J.A., Liebmann, B., Grimm, A.M., Misra, V., Silva Dias, P.L., Cavalcanti, I.F.A., Carvalho, L.M.V., Berbery, H., Ambrizzi, T., Vera, C.S., Saulo, A.C., Nogues Paegle, J., Zipser, E., Seth, A., Alves, L.M., 2012. Recent devel- opments on the SouthAmerican monsoon system. Int. J. Climatol. 32, 1–21. https://doi.org/10.1002/joc.2254.
Marengo Jr, J.A., Souza, C., Thonicke, K., Burton, C., Halladay, K., Betts, R.A., Alves, L.M., Soares, W.R., 2018. Changes in climate and Land use Over the Amazon region:current and future variability and trends. Front. Earth Sci. 6, 228. https://doi.org/10.3389/feart.2018.00228.
Martens, B., Miralles, D.G., Lievens, H., van der Schalie, R., de Jeu, R.A.M., Fernández-Prieto, D., Beck, H.E., Dorigo, W.A., Verhoest, N.E.C., 2017. GLEAM v3: satellite-based land evaporation and root-zone soil moisture. Geosci. Model Dev. 10, 1903–1925. https://doi.org/10.5194/gmd-10-1903-2017.
Miralles, D.G., Holmes, T.R.H., de Jeu, R.A.M., Gash, J.H., Meesters, A.G.C.A., Dolman, A.J., 2011. Global land-surface evaporation estimated from satellite-based observations. Hydrol. Earth Syst. Sci. 15, 453–469. https://doi.org/10.5194/hess-15-453-2011.
Molina-Carpio, J., Espinoza, J.C., Vauchel, P., Ronchail, J., Gutierrez, B., Guyot, J.L., Noriega, L., 2017. The hydroclimatology of the upper Madeira River basin: spatio-temporal variability and trends (1967–2013). Hydrol. Sci. J. https://doi.org/10.1080/02626667.2016.1267861.
Nobre, C.A., Sampaio, G., Borma, L.S., Castilla-rubio, J.C., Silva, J.S., Cardoso, M., 2016. Land-use and climate change risks in the Amazon and the need of a novel sustainable development paradigm. PNAS 113 (39), 10759–10768. https://doi.org/10.1073/pnas.16055. 16113.
Ovando, A., Tomasella, J., Rodriguez, D.A., Martinez, J.M., Siqueira-Junior, J.L., Pinto, G.L.N., Passy, P., Vauchel, P., Noriega, L., von Randow, C., 2016. Extreme flood events in the Bolivian Amazon wetlands. J. Hydrol. Regul. Stud. 5, 293–308.
Paccini, L., Espinoza, J.C., Ronchail, J., Segura, H., 2017. Intraseasonal rainfall variability in the Amazon basin related to large-scale circulation patterns: a focus on western Amazon-Andes transition region. Int. J. Climatol. https://doi.org/10.1002/joc.5341.
Paca, V.H.M., Espinoza-Davalos, G.E., Hessels, T.M., Moreira, D.M., Comair, G.F., Bastiaanssen, W.G.M., 2019. The spatial variability of actual evapotranspiration across the Amazon River Basin based on remote sensing products validated with flux towers. Ecol. Processes 8, 6. https://doi.org/10.1186/s13717-019-0158-8.
Paiva, R.C.D., Buarque, D.C., Collischonn, W., Bonnet, M.P., Frappart, F., Calmant, S., Bulhões Mendes, C.A., 2013. Large-scale hydrologic and hydrodynamic modeling of the Amazon River basin. Water Resour. Res. 49, 1226–1243.
Papa, F., Güntner, A., Frappart, F., Prigent, C., Rossow, W.B., 2008. Variations of surface water extent and water storage in large river basins: a comparison of different global data sources. Geophys. Res. Lett. 35 (11), L11401. https://doi.org/10.1029/2008GL033857.
Parrens, M., Al-Bitar, A., Frappart, F., Paiva, R.C.D., Wongchuig, C.S., Papa, F., Yamazaki, D., Kerr, Y., 2019. High resolution mapping of inundation area in the Amazon basin from a combination of L-band passive microwave, optical and radar datasets. Int. J. Appl. Earth. Obs. Geoinformation 81, 58–71. https://doi.org/10.1016/j.jag.2019.04.011.
Pettitt, A., 1979. A non-parametric approach to the change-point problem. Appl. Stat. 28, 126–135.
Polade, S.D., Pierce, D.W., Cayan, D.R., Gershunov, A., Dettinger, M.D., 2014. The key role of dry days in changing regional climate and precipitation regimes. Nat. Sci. Rep. 4, 4364. https://doi.org/10.1038/srep04364.
Ramillien, G., Famiglietti, J.S., Wahr, J., 2008. Detection of continental hydrology and glaciology signals from GRACE: a review. Surv. Geophys. 29, 361–374. https://doi.org/10.1007/s10712-008-9048-9.
Roche, M.A., et al., 1990. Hétérogénéité des précipitations sur la cordillère des Andes boliviennes. In: In: Lang, H. (Ed.), Hydrology in Mountainous Regions. Wallingford: International Association of Hydrological Sciences 193. IAHS Publication, pp. 381–388.
Rodell, M., Houser, P.R., Jambor, U., Gottschalck, J., Mitchell, K., Meng, C.J., Arsenault, K., Cosgrove, B., Radakovich, J., Bosilovich, M., Entin, J.K., Walker, J.P., Lohmann, D., Toll, D., 2004. The global land data assimilation system. B. Am. Meteorol. Soc. 85, 381–394. https://doi.org/10.1175/BAMS-85-3-381.
Ronchail, J., Gallaire, R., 2006. ENSO and rainfall along the Zongo Valley (Bolivia) from the altiplano to the Amazon basin. Int. J. Climatol. 26, 1223–1236. https://doi.org/10.1002/(ISSN)1097-0088.
Ronchail, J., Bourrel, L., Cochonneau, G., Vauchel, P., Phillips, L., Castro, A., Guyot, J.L., de Oliveira, E., 2005. Inundations in the Mamoré basin (south-western Amazon—Bolivia) and sea-surface temperature in the Pacific and Atlantic Oceans. J. Hydrol. 302, 223–238.
Saatchi, S., Asefi-Najafabady, S., Malhi, Y., LEOC, A., Anderson, L.O., Myneni, R.B., Nemani, R., 2013. Persistent effects of severe drought on Amazonian forest canopy. Proc. Natl. Acad. Sci. U. S. A. 110, 565–570. https://doi.org/10.1073/pnas.12046. 51110.
Sakumura, C., Bettadpur, S., Bruinsma, S., 2014. Ensemble prediction and intercomparison analysis of GRACE time-variable gravity field models. Geophys. Res. Lett. 41, 1389–1397.

Salazar, L.F., Nobre, C.A., Oyama, M.D., 2007. Climate change conse- quences on the biome distribution in tropical South America. Geophys. Res. Lett. 34 (9), L09708.
Siqueira, V.A., Paiva, R.C.D., Fleischmann, A.S., Fan, F.M., Ruhoff, A.L., Pontes, P.R.M., Paris, A., Calmant, S., Collischonn, W., 2018. Toward continental hydro- logic–hydrodynamic modeling in South America. Hydrol. Earth Syst. Sci. 22, 4815–4842.
Sörensson, A.A., Ruscica, R.C., 2018. Intercomparison and uncertainty assessment of nine evapotranspiration estimates over South America. Water Resour. Res. 54. https://doi.org/10.1002/2017WR021682.
Staal, A., et al., 2018. Forest-rainfall cascades buffer against drought across the Amazon. Nat. Clim. Change 8, 539–543. https://doi.org/10.1038/s41558-018-0177-y.
Sumila, T.C.A., Pires, G.F., Fontes, C.V., Costa, M.H., 2017. Sources of water vapor to economically relevant regions in Amazonia and the effect of deforestation. J. Hydromet. https://doi.org/10.1175/JHM-D-16-0133.1.
Sun, L., Baker, J.C.A., Gloor, E., Spracklen, D., Boesch, H., Somkuti, P., Maeda, E., Buermann, W., 2019. Seasonal and inter-annual variation of evapotranspiration in amazonia based on precipitation, river discharge and gravity anomaly data. Front. Earth Sci. 7, 32. https://doi.org/10.3389/feart.2019.00032.
Swenson, S., Wahr, J., 2006. Post-processing removal of correlated errors in GRACE data. Geophys. Res. Lett. 33 (8), 1–4. https://doi.org/10.1029/2005GL025285.
Tapley, B., Bettadpur, S., Ries, J., Thompson, P., Watkins, M., 2004. GRACE measurements of mass variability in the earth system. Science 305, 503–505. https://doi.org/10.1126/science.1099192.
Vera, C., et al., 2006. Towards a unified view of the American monsoon system. J. Clim. 19, 4977–5000.
Wongchuig-Correa, S., de Paiva, R.C.D., Espinoza, J.C., Collischonn, W., 2017. Multi-decadal hydrological retrospective: case study of amazon floods and droughts. J. Hydrol. https://doi.org/10.1016/j.jhydr. ol.2017.04.019.
Wu, J., Albert, L.P., Lopes, A.P., Restrepo-Coupe, N., Hayek, M., Wiedemann, K.T., et al., 2016. Leaf development and demography explain photosynthetic seasonality in Amazon evergreen forests. Science 351, 972–976.
Xavier, L., Becker, M., Cazenave, A., Longuevergne, L., Llovel, W., Rotunno Filho, O.C., 2010. Interannual variability in water storage over 2003–2008 in the Amazon basin from GRACE space gravimetry, in situ river level and precipitation data. Remote Sens. Environ. 114, 1629–1637. https://doi.org/10.1016/j.rse.2010.02.005.
Xu, Y., Wang, S., Bai, X., Shu, D., Tian, Y., 2018. Runoff response to climate change and human activities in a typical karst watershed, SW China. PLoS One 13 (3), e0193073. https://doi.org/10.1371/journal.pone.0193073.
Yoon, J.-H., Zeng, N., 2010. An Atlantic influence on Amazon rain- fall. Clim. Dyn. 34, 249–264. https://doi.org/10.1007/s0038. 2-009-0551-6.
Zbigniew, W., 2004. Change detection in hydrological records—a review of the methodology. Hydrol. Sci. J. 49, 7–119.
Zemp, D.C., Schleussner, C.F., Barbosa, H.M., Hirota, M., Montade, V., Sampaio, G., Staal, A., Wang-Erlandsson, L., Rammig, A., 2017. Self-amplified amazon forest loss due to vegetation-atmosphere feedbacks. Nat. Commun. 8 (14), 681.